Tellus (1996), 48B, 397–417
Printed in UK – all rights reserved

TELLUS
ISSN 0280–6509

An efficient and accurate representation of complex oceanic and biospheric models of anthropogenic carbon uptake

By FORTUNAT JOOS*[1], MICHELE BRUNO[2], ROGER FINK[3], ULRICH SIEGENTHALER‡ and THOMAS F. STOCKER[4], *Climate and Environmental Physics, Physics Institute, University of Bern, CH-3012 Bern, Switzerland*; CORINNE LE QUÉRÉ[5] and JORGE L. SARMIENTO[6], *Atmospheric and Oceanic Sciences Program, Princeton University, Princeton, NJ 08544–0710, USA*

(Manuscript received 28 August 1995; in final form 25 January 1996)

ABSTRACT

Establishing the link between atmospheric CO_2 concentration and anthropogenic carbon emissions requires the development of complex carbon cycle models of the primary sinks, the ocean and terrestrial biosphere. Once such models have been developed, the potential exists to use pulse response functions to characterize their behaviour. However, the application of response functions based on a pulse increase in atmospheric CO_2 to characterize oceanic uptake, the conventional technique, does not yield a very accurate result due to nonlinearities in the aquatic carbon chemistry. Here, we propose the use of an ocean mixed-layer pulse response function that characterizes the surface to deep ocean mixing in combination with a separate equation describing air-sea exchange. The use of a mixed-layer pulse response function avoids the problem arising from the nonlinearities of the carbon chemistry and gives therefore more accurate results. The response function is also valid for tracers other than carbon. We found that tracer uptake of the HILDA and Box-Diffusion model can be represented exactly by the new method. For the Princeton 3-D model, we find that the agreement between the complete model and its pulse substitute is better than 4% for the cumulative uptake of anthropogenic carbon for the period 1765 to 2300 applying the IPCC stabilisation scenarios S450 and S750 and better than 2% for the simulated inventory and surface concentration of bomb-produced radiocarbon. By contrast, the use of atmospheric response functions gives deviations up to 73% for the cumulative CO_2 uptake as calculated with the Princeton 3-D model. We introduce the use of a decay response function for calculating the potential carbon storage on land as a substitute for terrestrial biosphere models that describe the overturning of assimilated carbon. This, in combination with an equation describing the net primary productivity permits us to exactly characterize simple biosphere models. As the time scales of biospheric overturning are one key aspect to determine the amount of anthropogenic carbon which might be sequestered by the biosphere, we suggest that decay response functions should be used as a simple and standardized measure to compare different models and to improve understanding of their behaviour. We provide analytical formulations for mixed-layer and terrestrial biosphere decay pulse response functions which permit us to easily build a substitute for the "Bern" carbon cycle model (HILDA). Furthermore, mixed-layer response functions for the Box-Diffusion, a 2-D model, and the Princeton 3-D model are given.

[1]Tel.: +41-31-6314461; Fax.: +41-31-6314405; email: joos@climate.unibe.ch
[2]Tel.: +41-31-6314461; Fax.: +41-31-6314405; email: bruno@climate.unibe.ch
[3]Tel.: +41-31-6314461; Fax.: +41-31-6314405; email: fink@climate.unibe.ch
[4]Tel.: +41-31-6314462; Fax.: +41-31-6314405; email: stocker@climate.unibe.ch
[5]Tel.: +1-609-2581312; Fax.: +1-609-2582850; email: lequere@splash.princeton.edu
[6]Tel.: +1-609-2586585; Fax.: +1-609-2582850; email: jls@splash.princeton.edu
* Corresponding author.
‡ Deceased.

1. Introduction

Carbon cycle models that simulate the dynamics of the atmosphere–ocean–biosphere system are used for understanding the fate of anthropogenic CO_2, in particular how much of the carbon emitted into the atmosphere by burning fossil fuels and by land use has remained and will remain airborne. Calculation of atmospheric CO_2 concentrations from prescribed emissions, or vice versa, requires a substantial effort of model-building and computer programming, even for models of simple structure. The question of primary interest generally concerns the amount of excess carbon taken up by ocean and land biota. Instead of running a full carbon cycle model, this task can also be achieved using pulse response functions. As long as the carbon system behaves in an approximately linear way, the development of the atmospheric concentration for prescribed emissions is given by the convolution integral of the emission history with the atmospheric pulse response (Siegenthaler and Oeschger 1978, Oeschger and Heimann 1983, Maier-Reimer and Hasselmann, 1987, Sarmiento et al., 1992).

The dynamics of a linear system is fully characterized by its pulse response function (Green's function). The CO_2 system is approximately linear as long as the atmospheric concentration does not vary much. This allows one to use the response function of a carbon cycle model as a substitute for the full model for calculating the atmospheric concentration for a given emission history (or vice versa), a great simplification. Unfortunately, the nonlinearity of the CO_2 chemistry in the ocean limits the accuracy of this procedure significantly for CO_2 increases exceeding, $\sim 50\%$ of the pre-industrial level. The ratio between a change in partial pressure of CO_2 in seawater, ΔpCO_2, and total dissolved inorganic carbon, $\Delta\Sigma CO_2$, known as the buffer factor, increases with increasing pCO_2 levels. Consequently, the response function is different for emission pulses of different size or for pulses of the same size but emitted into an atmosphere with different CO_2 levels. In order to overcome this, Harvey (1989) and Wigley (1991) combined the pulse response functions of the Hamburg 3-dimensional ocean carbon model (Maier-Raimer and Hasselmann, 1987) for emission pulses of different sizes. This yields an improvement, but is still not fully satisfactory; the essential problem remains that the CO_2 system is non-linear because of the seawater chemistry.

We present a method which makes use of an ocean mixed-layer pulse response function to characterize ocean-atmosphere carbon cycle models. Mixed-layer pulse response functions as a means to represent ocean models have been introduced by Siegenthaler (1993). Here, we discuss the use of mixed-layer pulse response functions in detail and apply the method to the HILDA model (Joos et al., 1991; Joos, 1992; Siegenthaler and Joos, 1992),the Princeton 3-D model (Sarmiento et al., 1992) and a 2-D ocean model (Stocker et al., 1994). The method has 3 advantages. First, similar to the use of an atmosphere pulse response function, this method allows one to perform cost-effective calculations of the relationship between CO_2 emissions and atmospheric concentration for different scenarios. Second, it avoids the problem of non-linearities arising from seawater chemistry and therefore gives more accurate results. Third, it provides a simple measure of the surface to deep mixing and allows one to compare the behaviour of different ocean transport models. Finally, the oceanic response function can be applied not only to CO_2, but to any conservative tracer that has its source or sink in the atmosphere. For instance, this approach also permits one to study the oceanic uptake of bomb-produced radiocarbon, and approximately — for small temperature changes — even the heat uptake by the ocean, e.g. due to greenhouse warming (Bryan et al., 1983). In contrast, the atmospheric CO_2 pulse response is valid for CO_2 only.

Nonlinearities in carbon cycle models arise not only from the oceanic CO_2 uptake, but also from the description of the potential carbon storage on land due to fertilization by elevated CO_2 levels and nitrogen supply. As with air-sea exchange, net primary production is usually viewed as a nonlinear function of atmospheric CO_2. However, as with the transport within the ocean, the decay of living biomass into detritus, soil organic matter and back to atmospheric CO_2 may be approximated by a set of linear equations. We can therefore represent complex biosphere models by applying an equation describing net primary production and by calculating the decay of organic material as a function of past primary productivity and a "decay" pulse response function which gives

a measure of the mean overturning time of assimilated plant material.

This paper is organized as follows. Section 2 reviews the classical atmospheric pulse response function and presents the development of the mixed-layer pulse response function. Section 3 demonstrates the applicaton of mixed-layer pulse response functions to a hierarchy of global carbon cycle models of increasing complexity. The implementation of a simple biosphere model is discussed in Section 4 and the conclusion follows in Section 5. In the appendix, analytical representations of the pulse functions are given which allow one to build a substitute for the "Bern" carbon cycle model (the HILDA ocean model coupled to a 4-box biosphere; used by IPCC as the reference model for scenario calculations and the calculation of global warming potentials; IPCC, 1994), the Box-Diffusion model (Oeschger et al., 1975; Siegenthaler and Oeschger, 1987), a 2-D ocean model (Stocker et al., 1994) and the Princeton 3-D model (Sarmiento et al., 1992).

2. Pulse response functions

2.1. *Atmospheric pulse response function model*

Normalized atmospheric pulse response functions are usually obtained by monitoring the decrease of an atmospheric CO_2 perturbation due to an initial carbon input at time 0 using a full carbon cycle model. Fig. 1 shows different atmospheric pulse response functions for atmospheric CO_2 as obtained with the HILDA model. Its values depict the fraction of the initially added carbon which is still found in the atmosphere at any later time, i.e., the airborne fraction.

When considering the fate of anthropogenic CO_2, the emission into the atmosphere can be considered as a series of consecutive pulse inputs. The atmospheric CO_2 concentration $c_a(t)$ (in units of ppm) can then be represented as the sum of earlier emissions at times t', multiplied by the fraction still remaining airborne after time $t - t'$:

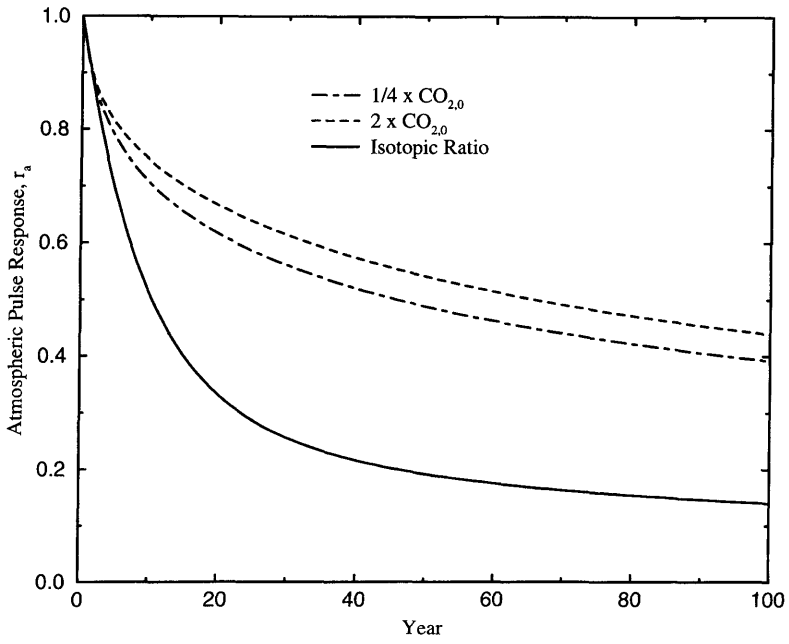

Fig. 1. Atmospheric pulse response functions for an isotopic ratio ($^{13}C/^{12}C$ or $^{14}C/^{12}C$) and for CO_2 as obtained by using the ocean-atmosphere compartments of the HILDA model with no biosphere. The response of the atmospheric CO_2 concentration to a pulse input depends on the pulse size and the CO_2 background concentration. The dashed line is for a doubling of preindustrial CO_2 concentration (280 ppm) at $t=0$; the dashed-dotted line is for an increase of pre-industrial CO_2 concentration by one quarter (70 ppm) at $t=0$; the solid line is for the decrease of an isotopic perturbation.

$$c_a(t) \approx \int_{t_0}^{t} e(t') r_a(t-t') dt' + c_a(t_0) \quad (\text{for } t \geq t_0). \tag{1}$$

The integral is evaluated for times t' between the time t_0 at which the atmospheric CO_2 concentration was found to be in equilibrium with the ocean and the biosphere (beginning of industrialization) and the time t at which the atmospheric concentration is calculated. The rate of CO_2 emissions, $e(t)$, is expressed in ppm yr^{-1} and $r_a(t)$ is the evolution of the airborne fraction due to a δ-function input at $t=0$ (atmospheric pulse response function). Here, as well as in the following paragraphs, the atmosphere is assumed to be well mixed, and a change in atmospheric concentration of 1 ppm is equivalent to a change in atmospheric carbon inventory of 2.123 10^{15} g C. Eq. (1) holds only approximately as will be discussed below. The definitions of e and r_a are related. If the pulse response function r_a is determined using a model which describes all removal processes of anthropogenic carbon from the atmosphere, the emission term e corresponds to the anthropogenic emissions. On the other hand, if r_a is determined using an ocean-atmosphere model only, the emission e corresponds to the difference of anthropogenic emissions minus other sink terms, namely the uptake of additional CO_2 by the biosphere. In the following, we focus on this latter application. Maier-Reimer and Hasselmann (1987) and Sarmiento et al. (1992) facilitated this approach by representing the atmospheric pulse response function of their 3-dimensional Ocean General Circulation Model as sums of exponential functions. We denote the use of eq. (1) to link CO_2 emissions and atmospheric CO_2 levels as the "atmospheric pulse response model" (or method).

Each response function in Fig. 1 has been obtained by monitoring the decay due to ocean uptake of an initial CO_2 input into the atmosphere for pulses of different magnitude. $r_a(t)$ depends on the pulse size and the CO_2 background level, because of the non-linearities of the seawater chemistry. This is the main disadvantage of the atmospheric pulse response model. In Fig. 2, oceanic CO_2 uptake rates as obtained by using the HILDA-model are compared with those obtained by the atmospheric pulse response method. In these experiments, atmospheric CO_2 concentrations are prescribed in order to stabilize its future values at 450 ppm (IPCC profile S450, Enting et al., 1994). Large deviations are found that seriously hamper the predictive value of such calculations. The cumulative ocean uptake as calculated by using the two atmospheric response functions is overestimated by 7% and 24% as compared to the results of the full HILDA model. One can find a particular atmospheric response function that gives more accurate results for a particular scenario, but it is not possible to obtain accurate results by applying one single response function to a variety of scenarios. By combining different atmospheric pulse response functions better results may be obtained as compared to a model using one response function only.

Another drawback of the atmospheric pulse response method is that atmospheric pulse response functions are in general different for different tracers. Several tracers are important to assess the global carbon cycle. For example, the atmospheric history of CO_2 and $^{13}CO_2$ allows one to discriminate between carbon fluxes into the ocean and into the land biosphere, (Keeling et al., 1989). The penetration of bomb-produced radiocarbon, or other transient tracers like CFCs is used to evaluate the transport scheme of ocean models (e.g., Oeschger et al. 1975; Toggweiler et al, 1989; Joos et al., 1991). Also included in Fig. 1 is the pulse response function for the decrease of a perturbation of the atmospheric $^{14}C/^{12}C$ ratio (or $^{13}C/^{12}C$) ratio. The isotopic perturbation decreases much more rapidly than a CO_2 perturbation. This is a consequence of different air-sea interactions (Heimann, 1993). The fraction of an initial perturbation remaining airborne is much higher for anthropogenic CO_2 than for a perturbation in the isotopic ratio. The oceanic CO_2 uptake is buffered by the sea water carbon chemistry; the relative change in the oceanic partial pressure of CO_2 is about $10\times$ larger than the relative change of the total dissolved inorganic carbon concentration. The isotopic ratio itself, however, is not, or only slightly, buffered. The difference between the pulse response functions for CO_2 and isotopic ratios demonstrates that there is in general no unique atmospheric pulse response function for different tracers.

2.2. *Mixed-layer pulse response function model*

The nonlinearity of the atmosphere-ocean CO_2 system resides in the transition from CO_2 to

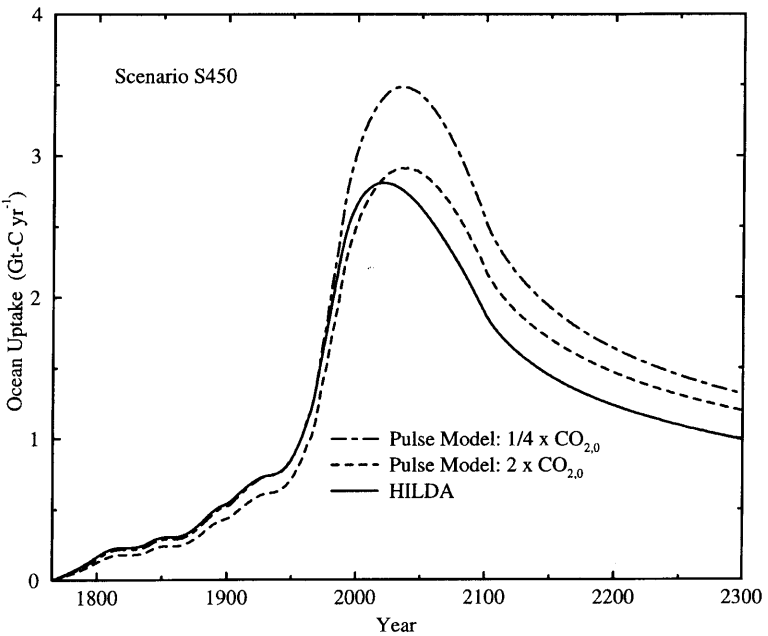

Fig. 2. Oceanic carbon uptake for IPCC scenario S450 as simulated with the HILDA model (solid line) and the atmospheric pulse response model using the response functions shown in Fig. 1. For the atmospheric pulse model, eq. (1) is solved simultaneously with the following mass balance equation: $e = dN_a/dt + dN_{oc}/dt$ which expresses that the emissions, e, are equal the change in atmospheric, dN_a/dt, and oceanic inventory, dN_{oc}/dt. Atmospheric CO_2 concentration and the change in atmospheric inventory is prescribed in order to stabilize concentration at 450 ppm (Enting et al., 1994).

HCO_3^- and CO_3^- that occurs when CO_2 dissolves in the ocean. The problem with this nonlinearity as well as the difference in air-sea exchange for different tracers can be overcome if instead of a CO_2 pulse input into the atmosphere we consider a pulse input into the surface ocean and treat the air-sea equilibration explicitly. The transport of excess CO_2 and of other passive tracers within the ocean is described as a set of linear equations and can therefore be exactly captured by pulse response functions.

To develop the basic idea, we first consider the pulse response substitution of an ocean model with one surface box only, e.g., the Box-Diffusion model. However, as we will see later the equations derived below are also valid for more complex ocean models. The surface water concentration (c_s) is given for an arbitrary time history of the atmosphere-ocean flux by:

$$c_s(t) = \frac{1}{h}\int_{t_0}^{t} f_{as}(t')r_s(t-t')\mathrm{d}t' + c_s(t_0), \quad (\text{for } t \geqslant t_0) \tag{2}$$

where h is the mixed-layer depth and $f_{as}(t)$ is the air-sea flux per unit area multiplied by the mixed-layer pulse response function r_s. In eq. (2) and in following eqs., the mixed layer is in equilibrium with the deep ocean at time t_0. The mixed-layer response function is a measure of the tracer removed by surface-to-deep mixing and represents the fraction of an initially added amount of tracer which is still found in the mixed layer after a certain time. It may be obtained by monitoring the decrease of a perturbation of the surface water concentration due to ocean circulation and mixing using an ocean transport model (air-sea exchange is set to zero). Eq. (2) is valid for any conservative tracer as long as ocean circulation, here represented by r_s, remains constant.

For carbon, we recast eq. (2) in the following form:

$$\begin{aligned}\delta\Sigma CO_2 &= \Sigma CO_2(t) - \Sigma CO_2(t_0) \\ &= \frac{c}{h}\int_{t_0}^{t} f_{as}(t')r_s(t-t')\mathrm{d}t',\end{aligned} \tag{3}$$

where $\delta\Sigma CO_2$ is the perturbation of dissolved inorganic carbon in surface water, e.g., due to the industrial CO_2 increase. A conversion factor c has been introduced to convert the air-sea flux from units of [ppm m^{-2} yr^{-1}] into units of [μmol m^{-2} yr^{-1}] and to convert m^3 into kg seawater (c = 1.722 10^{17} μmol m^3 ppm^{-1} kg^{-1}). To obtain the relationship between atmospheric CO_2 perturbation, $\delta pCO_{2,a}$, and carbon emissions, e, we make use of the following budget equation:

$$\frac{d}{dt}\delta pCO_{2,a} = e(t) - f_{as}(t)A_{oc} \quad (4)$$

(units for eq. 4: ppm yr^{-1}; Note that 1 ppm = 2.123×10^{15} g-C = 7.779×10^{15} g-CO_2 = 1.768 10^{14} mol) where A_{oc} is the ocean surface area. The emission term e includes any net fluxes into or out of the atmosphere except air-sea exchange. The net carbon flux between ocean and atmosphere, f_{as}, depends on the difference in partial pressure between surface ocean and atmosphere. Using a perturbation approach we may write:

$$f_{as}(t) = k_g(\delta pCO_{2,a} - \delta pCO_{2,s}), \quad (5)$$

where k_g represents the gas exchange coefficient related to the gas phase in units of [yr^{-1} m^{-2}], and δpCO_2 is the perturbation in the partial pressure in ppm. The relationship between the perturbation in dissolved inorganic carbon, obtained by solving eq. (3), and the partial pressure of surface ocean water used in eq. (5) may be obtained from the following analytical relationship which is good to within 1% for δpCO_2 smaller than 200 ppm (i.e., pCO2 < 480 ppm; Sarmiento et al., 1992):

for $0 < \delta pCO_{2,s} < 200$ ppm and $0°C < T < 30°C$:

$$\delta pCO_{2,s} = \frac{z_0 \delta\Sigma CO_2}{1 - z_1 \delta\Sigma CO_2}, \quad (6a)$$

where

$$z_0 = 1.7561 - 0.031618 \times T + 0.0004444 \times T^2$$

and

$$z_1 = 0.004096 - 7.7086 \times 10^{-5} \times T + 6.10 \times 10^{-7} \times T^2,$$

where δpCO_2 is in units of ppm, $\delta\Sigma CO_2$ in μmol kg^{-1}, and T in °C (Note, there was a typesetting error in the equation for z_0 in the original publication). To derive this parameterization, ocean surface water is assumed to be in equilibrium with an atmospheric CO_2 concentration of 280 ppm everywhere and to have a uniform alkalinity of 2300 μeq kg^{-1}.

For the pulse models, we have extended the above parameterization for the global average surface water temperature as used in various models up to δpCO_2 values of 1320 ppm and pCO_2 values of 1600 ppm using the equilibrium constants of Roy et al. (1993) and Goyet and Poisson (1989) as summarized by Millero (1995). The following expression is good to within 0.1%:

for $0 \leq \delta pCO_{2,s} \leq 1320$ ppm

and $17.7°C \leq T \leq 18.3$ °C:

$$\begin{aligned}\delta pCO_{2,s} = {} & (1.5568 - 1.3993 \times 10^{-2} \times T) \times \delta\Sigma CO_2 \\ & + (7.4706 - 0.20207 \times T) \times 10^{-3} \\ & \times (\delta\Sigma CO_2)^2 \\ & - (1.2748 - 0.12015 \times T) \\ & \times 10^{-5} \times (\delta\Sigma CO_2)^3 \\ & + (2.4491 - 0.12639 \times T) \times 10^{-7} \\ & \times (\delta\Sigma CO_2)^4 \\ & - (1.5468 - 0.15326 \times T) \\ & \times 10^{-10} \times (\delta\Sigma CO_2)^5. \end{aligned} \quad (6b)$$

Again δpCO_2 is in units of ppm, $\delta\Sigma CO_2$ in μmol kg^{-1}, and T in °C.

If the oceanic response function $r_s(t)$ is known, eqs. (3)–(6) can be solved simultaneously to obtain the atmospheric CO_2 increase given prescribed carbon emissions or vice versa. The nonlinearity of the CO_2 chemistry is now contained in the expression for δpCO_s (eq. (5) and (6)), while the response function $r_s(t)$ is independent of the size of the CO_2 perturbation. The dependence of the atmospheric pulse response on the size of the CO_2 increase is incorporated in $f_{as}(t)$.

Since the surface-to-deep mixing is tracer independent, the ocean pulse response function is valid for any passive tracer. For example, to calculate the oceanic uptake of bomb-produced radiocarbon, we replace the equation describing air-sea exchange for carbon (eq. (5)) by:

$$^{14}f_{as}(t) = k_g \times pCO_{2,a}(^{14}R_a - ^{14}R_s) - ^{14}f_{as}(1950); \quad (7)$$

here, ^{14}R represents the fractionation corrected atomic ratio $^{14}C/^{12}C$. We prescribe atmospheric CO_2 and radiocarbon levels and use eq. (2) to calculate the radiocarbon ratio of the surface layer. In general, oceanic uptake of different tracers can be calculated by using the same mixed-layer pulse response function.

The approach outlined above is exact for ocean models with only one surface box. For models with higher spatial resolution the situation is more complex. The surface layer of the HILDA model consists of two well-mixed boxes, one representing low and mid-latitude surface water (LS-box) and the other representing high-latitude water masses (HS-box). To correctly describe the air-sea exchange, fluxes need to be considered separately for each surface box. For the moment, we consider exchange fluxes with the LS-box only. The concentration in the LS-box (c_{LS}) is given by analogy with eq. (2) as:

$$c_{LS}(t) = \frac{1}{h}\int_{t_0}^{t} f_{a\text{-}LS}(t')r_{LS}(t-t')\mathrm{d}t + c_{LS}(t_0). \quad (\text{for } t \geqslant t_0 \text{ and } f_{a\text{-}HS}=0) \tag{8}$$

Here, $f_{a\text{-}LS}$ represents the flux between the LS-box and the atmosphere. The response function for the LS-box, r_{LS}, is obtained by monitoring the decrease of an initial pulse into the LS-box while setting the air-sea exchange to zero. After a pulse input into the LS-box, the concentration of the HS-box will increase due to transport between the LS-and HS-boxes. The concentration in the HS-box normalized by the initial perturbation in the LS-box defines then a "transfer" pulse response function, $r_{LS,HS}$. The concentration in the HS-box is then given for a case with air-sea exchange for the LS-box only by:

$$c_{HS}(t) = \frac{1}{h}\int_{t_0}^{t} f_{a\text{-}LS}(t')r_{LS,HS}(t-t')\mathrm{d}t + c_{HS}(t_0) \quad (\text{for } t \geqslant t_0 \text{ and } f_{a\text{-}HS}=0). \tag{9}$$

Similarly, one may now define for the HS-box only a pulse response function, r_{HS}, and a transfer pulse response function, $r_{HS,LS}$. As ocean transport is linear, the surface concentrations resulting from the combined flux into both the LS and HS-box can be represented by superimposing the impact of air-sea exchange for both surface reservoirs:

$$c_{LS}(t) = \frac{1}{h}\int_{t_0}^{t} [f_{a\text{-}LS}(t')r_{LS}(t-t') + f_{a\text{-}HS}(t')r_{HS,LS}(t-t')] \times \mathrm{d}t' + c_{LS}(t_0) \quad (\text{for } t \geqslant t_0) \tag{10}$$

$$c_{HS}(t) = \frac{1}{h}\int_{t_0}^{t} [f_{a\text{-}HS}(t')r_{HS}(t-t') + f_{a\text{-}LS}(t')r_{LS,HS}(t-t')] \times \mathrm{d}t' + c_{HS}(t_0) \quad (\text{for } t \geqslant t_0). \tag{11}$$

The air-sea exchange for the two surface boxes, $f_{a\text{-}LS}$ and $f_{a\text{-}HS}$ and the concentration change in the atmosphere can then be calculated similarly as described in the previous paragraphs (eq. (3–6)).

In principle, this approach can be extended for models with more surfaces boxes. The concentration of surface box j is given by:

$$c_j(t) = \frac{1}{h}\int_{t_0}^{t} \mathrm{d}t' \left[\sum_{i=1}^{n} f_{a\text{-}i}(t')r_{ij}(t-t')\right] + c_j(t_0), \quad (\text{for } t \geqslant t_0) \tag{12}$$

where $f_{a\text{-}i}$ is the air-sea flux for surface box i, and r_{jj} for $i=j$ is the pulse response function for box j with respect to a flux into the same box j, and r_{ij} for $i \neq j$ are the transfer pulse response functions for reservoir j with respect to fluxes into other surface boxes. For an exact representation of a model with n surface boxes, one would in principle need n simulations to determine n^2 pulse response functions. This means that for general circulation models with typically $> 10^3$ surface boxes, an exact representation is not feasible. However, one may consider averages over many grid boxes to reduce the amount of equations needed. For example, by averaging eq. (12) over the whole ocean, we obtain for the globally averaged surface water concentration, $\bar{c}_s$:

$$\bar{c}_s(t) = \frac{1}{h}\int_{t_0}^{t} \mathrm{d}t' \bar{f}_{a\text{-}s}(t')\bar{r}_s(t-t') + \frac{1}{h}\int_{t_0}^{t} \mathrm{d}t' \left(\sum_{i=1}^{n} f'_{a\text{-}i}(t') \sum_{j=1}^{n} r_{ij}(t-t') \frac{A_j}{A_{oc}}\right) + c_s(t_0) \tag{13}$$

To derive eq. (13), we have expressed the air-sea flux for box i by the global average value $\bar{f}_{a\text{-}s}$, and its local deviation from this average, $f'_{a\text{-}i}$. A_j is the area covered by surface box j and the global mixed-layer pulse response function, $\bar{r}_s$ is defined as the area weighted sum over all local pulse

response functions. The first integral of eq. (13) corresponds to eq. (2). The second integral gives the deviations from the full model which arise from the nonlinear coupling of the spatially variable air-sea exchange ($f'_{a\text{-}i}$) and ocean transport (here represented by r_{ij}).

As long as the second integral of eq. (13) is small, even a complex model can be represented with good accuracy by a single mixed-layer pulse response function ($\bar{r}_s$). Then, eqs. (3) to (6) might also be used to approximate the behaviour of a complex OGCM by interpreting the variables used in these equations ($\delta\Sigma CO_2$, δpCO_2, f_{as}, r_s, T, etc) as global average values. The success of the approach will be examined below.

3. Validation

3.1. *HILDA model*

We first compare results obtained with the complete HILDA-model and with its representation in terms of ocean pulse response functions. For the latter, we use the 4 pulse response functions shown in Fig. 3 and as given in the appendix. These functions have been determined by using the full HILDA model. As an example, we monitor the atmospheric CO_2 concentration after a doubling of the preindustrial concentration. In the HILDA-model, a time step of 0.01 year was applied to integrate the model using a forth-order Runge-Kutta scheme. For the pulse response model, the integral in eq. (3) is represented as a sum using an interval of 0.01 year and 0.1 year. Deviations between the results of the pulse model and of the full HILDA model were smaller than 0.03% when a time step of 0.01 year was applied in the pulse model and 0.15% for a time step of 0.1 year. These deviations are due to the different numerical representation used in the two models. Similarly accurate results of the pulse response function model were also found for other scenarios linking emissions and atmospheric CO_2 as well as for the uptake of bomb-produced radiocarbon. This demonstrates that box-models of simple structure can be represented with good accuracy by the ocean pulse response function method using a relatively large time step of 0.1 year and a simple numerical representation. The pulse model runs about 60 times faster than the HILDA model.

3.2. *Princeton general circulation ocean model*

In a first experiment, the mixed-layer pulse response function is obtained by following the release of a passive tracer. Air-sea exchange is set to zero and the tracer concentrations are initialized to 1 in all surface boxes and 0 elsewhere. Monitoring the decrease of the globally averaged surface concentration due to mixing yields the globally averaged "tracer" mixed-layer pulse response function, $\bar{r}_s$ (Fig. 4).

The tracer mixed-layer pulse response function in combination with eqs. (3)–(6) is then used to calculate the oceanic uptake for the IPCC stabilization profiles S450 and S750. In these simulations the atmospheric concentrations are prescribed. To calculate the relationship between δpCO_2 and $\delta\Sigma CO_2$, the globally averaged surface temperature (17.7 °C) is used in eq. (6a). A comparison with the results obtained by running the full model shows that the ocean uptake in the pulse model is about 10% too low. Similarly, a too sluggish surface to deep mixing is found in a pulse simulation for the uptake of bomb-produced radiocarbon. This leads to an underestimation of the global bomb radiocarbon inventory of about 6% as compared with the full model results. As pointed out above, nonlinearities arising from the spatial variability of air-sea exchange and local transport (second integral in eq. (12)) lead to these deviations between the pulse substitute and the full 3-D model. Although these deviations are large, they are still substantially smaller than the uncertainties of oceanic CO_2 uptake or of the estimates of the bomb-radiocarbon inventory based on observations (Broecker et al., 1985). Nevertheless, these deviations between 3-D model and pulse model are not very satisfying.

To improve the agreement between the two models, we have applied a second method to calculate mixed-layer pulse response functions. We have calculated an "effective" mixed-layer pulse response function for the Princeton 3-D model by deconvolving the results of an existing atmospheric pulse response experiment (pulse size of 265 ppm; Sarmiento et al. 1992). Eqs. (3), (5), and (6) are solved for the unknown mixed-layer response, r_s, by using the atmospheric CO_2 perturbation, $\delta pCO_{2,a}$, and the net air-sea flux, f_{as}, as calculated with the full model. This approach has the advantage that nonlinearities arising from the local inter-

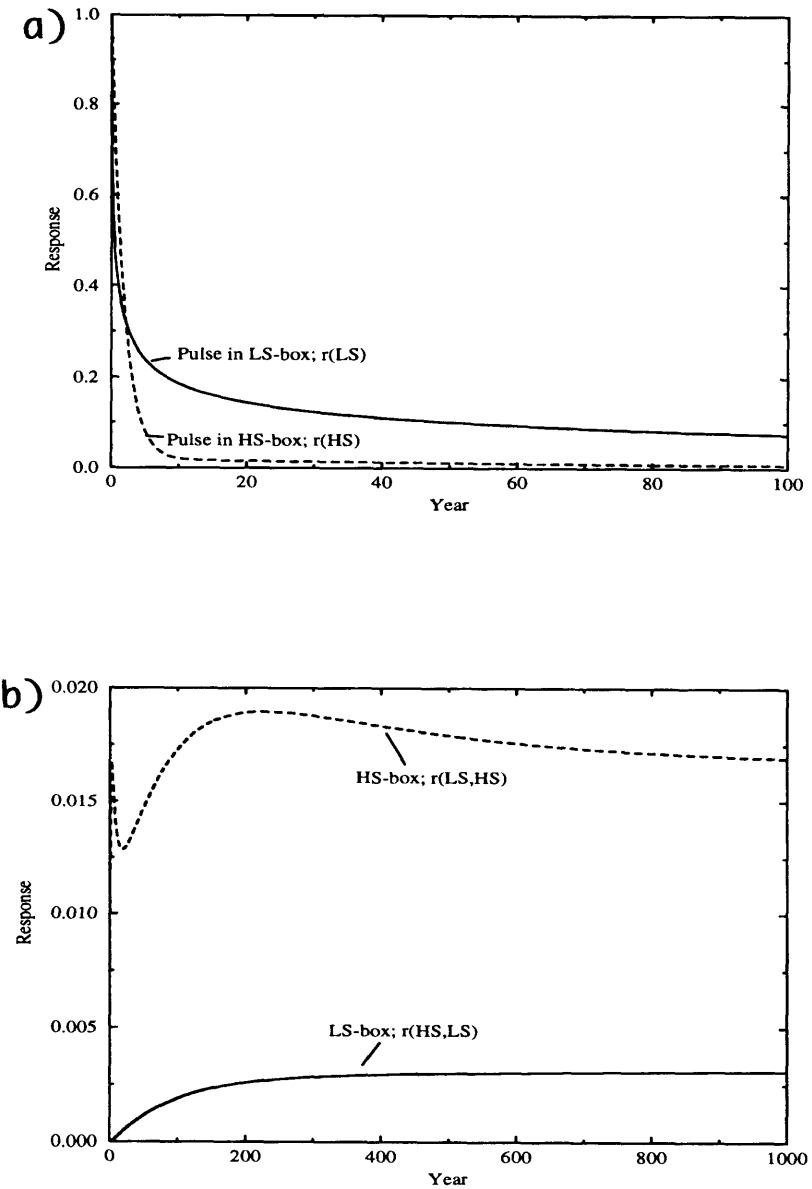

Fig. 3. Response of the concentrations in the two surface reservoirs of the HILDA model after a pulse input at $t=$ 0 into the low latitude surface box (LS) and the high-latitude surface box(HS), respectively. Concentrations are normalized to the initial tracer concentrations in the LS and HS-box. (a) Concentration change in the LS (solid line) and HS-reservoir (dashed line) due to a pulse input into each box. (b) Transfer pulse response functions for the two reservoirs. The solid line is for the concentration change in the LS-box due to a pulse input into the HS-box; the dashed line is for the concentration change in HS-box due to input into the LS-box. Note that different scales are used in (a) and (b).

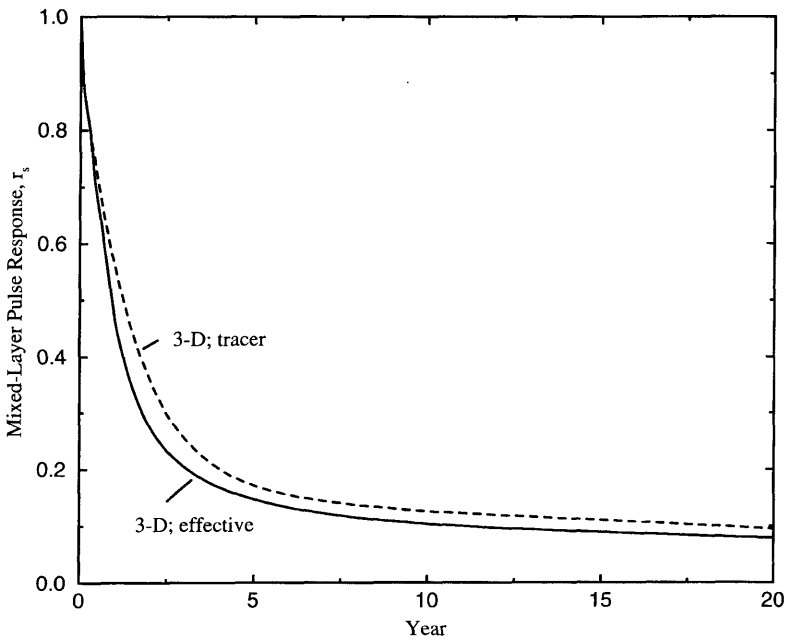

Fig. 4. Mixed-layer response functions as determined for the Princeton 3-D model. The tracer mixed-layer response (dashed curve) was obtained by monitoring the decrease of the globally averaged mixed-layer concentration due to ocean transport with tracer concentration initialized to 1 in the surface layer and to 0 everywhere else. Air-sea exchange was set to zero. The effective response (solid line) was calculated by prescribing atmospheric CO_2 and the net air-sea flux as obtained from an atmospheric pulse experiment and then deconvolving eq. (3)–(6) to determine the mixed layer function . In this way, non-linearities arising from local variability of the air-sea flux and surface to deep mixing are partly taken into account. This yields lower values corresponding to an apparently faster mixing for the effective response as compared to the results obtained from the mixed-layer tracer experiment.

play of air-sea exchange and mixing are implicitly taken into account. A fit of the calculated effective response function is provided in the appendix. We have checked the effective function obtained by deconvolving the results of two additional atmospheric pulse experiments (pulse size: 66.25 ppm and 795 ppm). To relate pCO_2 and ΣCO_2 in surface water, the globally averaged surface layer temperature of 17.7 °C is used in eq. (6a). The effective response function shown in Fig. 4 and as given in the appendix describes a faster surface to deep mixing as compared to the tracer pulse function obtained by the mixed-layer pulse experiment. This is due to the fact that the flux into the ocean occurs predominantly in oceanic regions of rapid vertical exchange (see Sarmiento et al., 1992).

The effective mixed-layer pulse response function has been used in several experiments. Fig. 5a compares air-sea fluxes as obtained by using the pulse reponse model and the Princeton 3-D model for the IPCC stabilization profiles S450 and S750 (Sarmiento et al, 1995). In Fig. 6 the ocean inventory and surface concentration of bomb-produced radiocarbon are shown for the two models. The agreement between the effective pulse model and the Princeton model is improved over that obtained with the tracer mixed-layer pulse model. To investigate the performance of the mixed-layer approach and that of the atmospheric pulse model, we compare the cumulative ocean uptake of anthropogenic CO_2 as obtained by running the full 3-D model, the mixed-layer pulse model using the effective response function as well as by three versions of the atmospheric pulse model. For the latter, atmospheric CO_2 pulse response functions are obtained from 3-D pulse experiments using pulse sizes of 66.25, 265 and 795 ppm (Sarmiento et al., 1992). The comparison reveals the large improvement in accuracy when applying the effective mixed-layer pulse method as compared

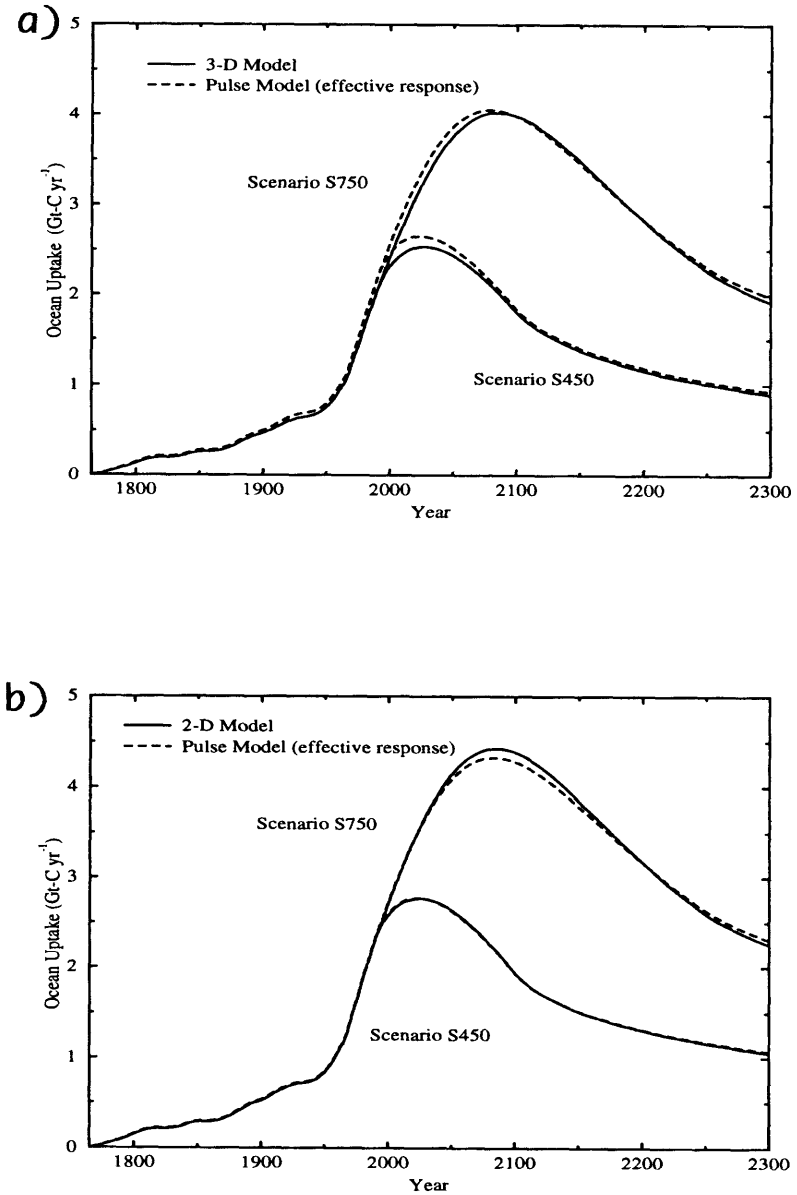

Fig. 5. (a) Oceanic carbon uptake for two different scenarios as simulated with the Princeton 3-D carbon cycle model (solid line) and the effective mixed-layer pulse response function (dashed line) shown in Fig. 4. Atmospheric CO_2 concentrations are prescribed in order to stabilize concentration at 450 and 750 ppm (IPCC stabilization profiles S450 and S750; Enting et al., 1994; Sarmiento et al., 1995). (b) As in (a) but showing results from the 2-D model of Stocker et al. (1994).

to the atmospheric pulse model (Table 1). For each of the considered 4 time intervals, results for the cumulative ocean uptake agree with the 3-D results within 6% or better for the effective mixed-layer pulse model, whereas deviations as large as 105% are found when applying the atmospheric pulse model (Table 1). This demonstrates that results obtained by using an atmospheric pulse

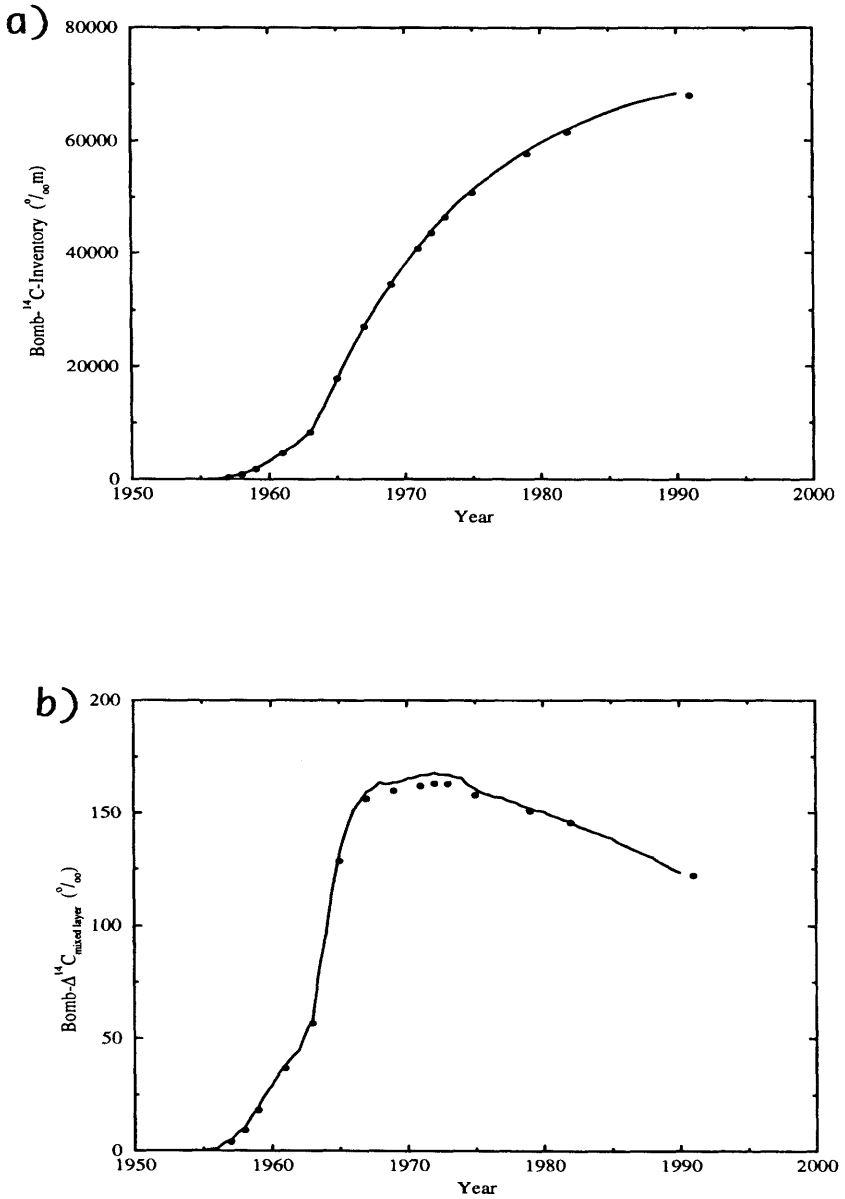

Fig. 6. (a) Oceanic bomb-radiocarbon inventory and (b) globally averaged surface concentration of bomb-produced radiocarbon as obtained with the mixed-layer pulse response model using the effective pulse response function (solid line) and the Princeton 3-d carbon cycle model (dots; J. Orr, personal communication). The increase in atmospheric radiocarbon ($\delta^{14}R_a$) due to the bomb tests is prescribed according to observations. The air-sea flux in surface box j is calculated as $f_{as}(t,j)=k_g\ pCO_{2,a}(t)^*(\delta^{14}R_a(t)-\delta^{14}R_s(t,j))$, thus the term $k_g^*(pCO_{2,a}(t)-pCO_{2,a}(1950)\times(\delta^{14}R_a(1950)-\delta^{14}R_s(1950j))$ is neglected.

Table 1. *Comparison between results of the full Princeton 3-D model, the mixed-layer pulse model using the effective response function of the 3-D model provided in the appendix, and the results of three versions of the atmospheric pulse response model; for the latter, the atmospheric response functions were obtained from three different 3-D pulse simulations using a pulse size of 66.25 ppm, 265 ppm, and 795 ppm (Sarmiento et al, 1992); for the stabilization scenarios S450 and S750, the cumulative oceanic uptake of anthropogenic CO_2 is given in Gt-C for four different periods; deviations between the pulse models and the 3-D model are shown in percent*

Period/ model	1765–1990 Gt-C	deviation	1990–2100 Gt-C	deviation	2100–2300 Gt-C	deviation	1765–2300 Gt-C	deviation
			Scenario S450					
3-D model	114		253		241		608	
mixed-layer pulse model	121	6%	263	4%	246	2%	630	4%
atmospheric pulse model								
size = 66.25 ppm	117	3%	327	29%	328	36%	772	27%
size = 265 ppm	98	−14%	276	9%	292	21%	666	10%
size = 795 ppm	64	−44%	183	−28%	208	−14%	455	−25%
			Scenario S750					
3-D model	114		381		574		1069	
mixed-layer pulse model	121	6%	392	3%	577	0.5%	1090	2%
atmospheric pulse model								
size = 66.25 ppm	117	3%	554	45%	1176	105%	1847	73%
size = 265 ppm	98	−14%	465	22%	1019	76%	1582	48%
size = 795 ppm	64	−44%	307	−19%	700	+22%	1071	0.2%

response model must be interpreted with caution, expecially when considering large deviations from equilibrium.

Two further issues with respect to the carbon chemistry implementation must be addressed. First, Sarmiento et al. (1995) have used the chemistry parameterization as defined by eq. (6a) also for scenario S750, where the parameterization is not as accurate for high CO_2 levels as for values below 500 ppm. The oceanic uptake for Scenario S750 is about 5% less than estimated with the effective pulse model in combination with the chemistry parameterization of eq. (6b).Second, the perturbation approach by definition neglects the spatial and temporal variability of alkalinity and pCO_2 in surface water which are due to the natural carbon cycle. Thus, the chemistry equations are evaluated for constant partial pressure (280 ppm) and alkalinity (2300 $\mu eq\ kg^{-1}$).

3.3. 2-D model

As an additional check of the pulse response approach and to address the effect of variable surface pCO_2 levels, we ran experiments using the dynamical 2-dimensional ocean circulation model of Stocker et al. (1994, circulation state A). First, carbon was implemented into the model using the perturbation approach of Sarmiento et al. (1992). Thus, eq. (6a) is used to describe the relationship between CO_2 partial pressure and inorganic carbon content of surface waters. For this perturbation model, the effective response is determined from a doubling CO_2 experiment (pulse size: 280 ppm). As for the 3-D model, we find a good agreement between the full model and pulse model results for scenario S450 and S750. For S750, the deviations are largest at the maximum uptake (5%) in 2075 and tend toward zero for years greater than 2200; for S450 deviations are negligible.

The same experiments were carried out again with the inorganic carbon model of Stocker et al. to investigate the effect of a locally variable surface water pCO_2 (1994). As a modification, here average ocean alkalinity is set equal to the average surface value of 2303 $\mu eq\ kg^{-1}$ (2373 $\mu eq\ kg^{-1}$ in Stocker et al., 1994). For the latter case, surface alkalinity, and thus CO_2 uptake, is slightly overpredicted, as $CaCO_3$ sedimentation is not included in the inorganic model. Surface water concentration of dissolved inorganic carbon is explicitly

calculated from the tracer conservation equations, and the partial pressure of CO_2 is allowed to vary locally. However, variations due to marine biological activities are neglected as well. The effective pulse response function is determined for the inorganic model, using again results of a doubling CO_2 pulse experiment (see Appendix). In Fig. 5b, results of the inorganic model and the pulse response model are compared. For the pulse model, carbon chemistry is parameterized according to eq. (6b). Again, we find good agreement between the full inorganic model and its pulse substitute. This means, that the effective pulse function approach is also valid for models which include the spatial variability of the CO_2 partial pressure due to natural processes. Despite the fact that the pulse model makes use of a perturbation chemistry, it is able to reproduce the overall behaviour of the inorganic 2-D model including the complete chemistry.

3.4. Comparison of mixed-layer pulse response functions

The mixed-layer pulse response function gives a measure of the intensity of surface-to-deep mixing of an ocean model. In Fig. 7a the effective pulse response functions as obtained for the the Box-Diffusion model, the HILDA model, the 2-D model and for the Princeton ocean general circulation model are compared. After an initial tracer injection, the concentration in the surface layer decreases very rapidly due to transport to depth. On a much longer time scale, a final equilibrium is reached when the tracer is mixed relatively uniformly throughout the whole ocean. A major difference between the 2-D and 3-D model versus the B-D and the HILDA models is the equilibrium values. This is due to the different surface layer depths of the individual models. The surface layer in the 2-D and 3-D models has a depth of about 50 meters, whereas the mixed layer in the HILDA and box-diffusion models is 75 m thick. Therefore, the same air-to-sea flux changes the concentraction in the mixed layers of the box-type models only by about 2/3 as compared with the two dynamical models. Thus, differences in the equilibrium values of the pulse response functions are largely due to different surface-to-deep ocean volume ratios in the individual models. To compare the model behaviour for long time scales (>20 years), we scale the response function by normalizing it to a mixed layer depth of 50 m (Fig. 7b). The scaled long-term responses are nearly identical (0.001 units dev. maximum) for HILDA, and 3-D models but consistently smaller for the box-diffusion and the 2-D model (0.005 units). The lower values for the box-diffusion model are due to the absence of a cold surface water mass. In chemical equilibrium, cold water masses take up less anthropogenic CO_2 than warm waters, thus the BD-model with its uniform warm surface layer absorbs more anthropogenic CO_2.

Differences between the pulse response functions in the first years reflect truly different dynamical behaviour of the ocean models. However, only models with approximately the same surface layer depth can be compared directly. This is the case for the 2-D and 3-D model. The initial mixing in the 2-D model is faster than in the 3-D model (Fig. 7a). Consequently, the uptake of anthropogenic CO_2 is larger for the 2-D model (air-sea flux at 1990.5: 2.34 Gt-C yr^{-1}) than for the 3-D (2.07 Gt-C yr^{-1}).

4. Coupling of a biosphere model

For simplification of scenario calculations linking atmospheric CO_2 and anthropogenic emissions, we need to consider the possible uptake of anthropogenic carbon by the biosphere due to a potential stimulation of plant growth by elevated CO_2 levels and enhanced nutrient supply (IPCC, 1994). The emission term e in eq. (4) may be subdivided into anthropogenic emissions, — including emissions by fossil fuel combustion, cement production, deforestation and land use changes —, and an additional biospheric sink term, f_{fer}:

$$e = e_{anthropogenic} - f_{fer} \tag{14}$$

To calculate the biospheric fertilization, f_{fer}, one may either couple a full biosphere model to the mixed-layer pulse model (eqs. (3)–(6)), or represent the biospheric uptake considering an atmospheric pulse response function. A third approach is to apply a technique analogous to that used for the the oceanic uptake by which pulse inputs into living biomass rather than into the atmosphere are considered.

One can calculate an atmospheric pulse

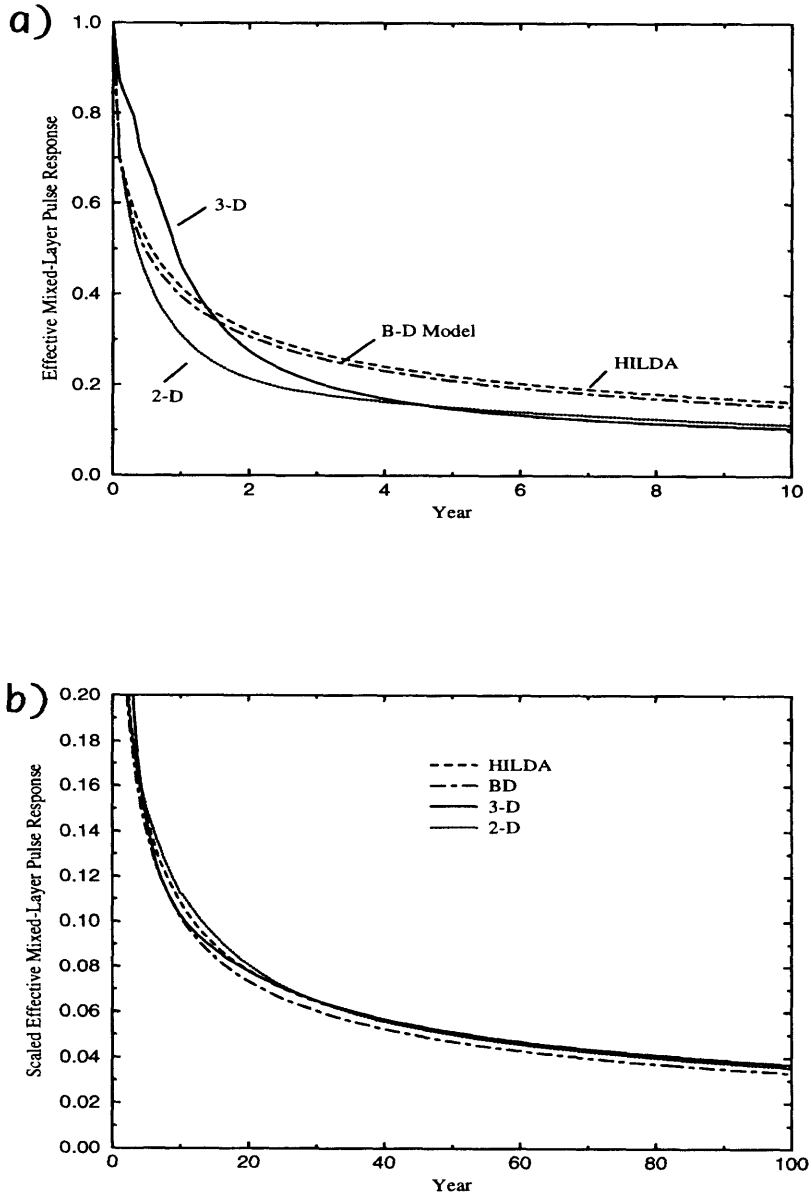

Fig. 7. (a) Effective mixed-layer pulse response functions for the Box-Diffusion model (dash-dotted), the HILDA model (dashed), the 2-D model (dotted), and the Princeton general circulation model (solid line) as obtained by deconvolving the full model results of an atmospheric pulse experiment. (b) The same mixed-layer response functions as shown in Fig. 7a, but normalized to a mixed-layer depth of 50 m. The effective response functions have been multiplied by 50 m and divided by the models' mixed-layer thickness.

response function for an atmosphere-biosphere carbon cycle model as has been done for ocean-atmosphere models. This response function, $r_{a:bio}$, describes the removal of atmospheric carbon into the biosphere. The additional biospheric storage is the difference between the carbon incorporated into living biomass (net primary production) and the decay of organic material. The response func-

tion may be used to calculate the fertilization term in eq. (14) with the help of:

$$CO_{2,a}(t) \approx \int_{t_0}^{t} (e_{anthrop}(t') - f_{as}(t') \times A_{oc}) r_{a:bio}(t-t')dt' + CO_{2,a}(t_0) \quad (\text{for } t \geq t_0). \tag{15}$$

As pointed out by Enting et al. (1994), the atmospheric pulse response functions describing air-sea uptake, $r_{a:oc}$, and biospheric uptake, $r_{a:bio}$, may be combined to obtain an overall atmospheric pulse response function for the coupled biosphere-atmosphere-ocean model.

Eq. (15) is exactly valid for linear atmosphere-biosphere models only. However, as for air-sea exchange, the additional net primary production as stimulated by elevated CO_2 levels and nutrient supply is often described by non-linear equations. On the other hand, the decay of the added biomass may be described by a set of linear equations assuming different biospheric carbon pools and turnover rates and can thus be fully characterized by a pulse response function. However, it should be noted that turnover rates depend on temperature and humidity and thus the equations describing the decay of organic matter are only linear under the assumption of a constant climate. In such a case, it seems natural to describe the additional net primary production and decay of biospheric material separately, i.e.,

$$f_{fer}(t) = \delta f_{npp} - \delta f_{decay} = \delta f_{npp}(t) - \int_{-\infty}^{t} \delta f_{npp}(t') r_{decay}(t-t')dt', \tag{16}$$

here δf_{npp} and δf_{decay} describe the additional net primary production and decay of organic material due to fertilization alone. The latter is a function of surplus primary production at earlier times and the response function, r_{decay}, which describes the turnover time of the photosynthesized carbon. The "decay response function", r_{decay}, may be calculated analytically, or by monitoring the biosphere-to-atmosphere flux after an initial injection of carbon into the assimilation pool(s). Furthermore, it may be obtained from any experiment with known primary production and return flux to the atmosphere by using eq. (16).

As an example, we use eq. (16) to substitute for the biospheric component of the "Bern" carbon cycle model. This model biosphere consists of four pools representing ground vegetation, wood, detritus and soil organic carbon (Emanuel et al., 1984; Siegenthaler and Oeschger, 1987) with each reservoir having a distinct overturning time (2.9, 20, 2.2, and 100 years). The net biosphere-to-air carbon flux due to decay of carbon added by the fertilization term is a function of these four overturning times. It increases after the time of the injection of additional carbon into the assimilation pools to reach its maximum about 2.7 years later and then decreases again and eventually disappears. This decay response function is shown in Fig. 8 and represented analytically in the appendix.

For the version of the "Bern" carbon cycle model which was used to perform the scenario calculations for IPCC, it has been assumed that the net primary productivity depends logarithmically on atmospheric CO_2 (Enting et al., 1994):

$$\delta f_{npp}(t) = 60\text{Gt-C yr}^{-1} \times \beta \ln(CO_{2,a}(t)/278 \text{ ppm}). \tag{17}$$

The value of β (=0.287), the so called fertilization factor, is adjusted in order to balance the anthropogenic CO_2 budget during the 80's assuming an average net deforestation flux of 1.1Gt-C yr^{-1} for the last decade (Note that for the IPCC 1994 report $\beta = 0.38$ has been used to balance a deforestation source of 1.6 Gt-C yr^{-1}). Eq. (17) is a great simplification of the actual processes and is only justified by the lack of better knowledge.

In more complex models, respiration and the turnover of assimilated carbon is not only a function of pool sizes but also of air temperature, soil temperature and soil humidity (e.g., Esser, 1987; Lüdeke et al., 1994, McGuire et al., 1992, Parton et al., 1987). Thus, the decay of assimilated carbon depends on climate which might change in the near future as a consequence of global warming. The assumption of a linear relationship for carbon respiration might therefore not be valid anymore. The validity and limitations of a pulse model to describe complex biosphere models need to be tested in the future.

5. Conclusion

The behavior of tracer uptake in simple box-diffusion models as well as complex general circulation ocean models can be represented by only a few equations in combination with a mixed-layer pulse response function. Such a pulse model can be used to calculate the oceanic uptake of any conservative (and passive) tracer which has its

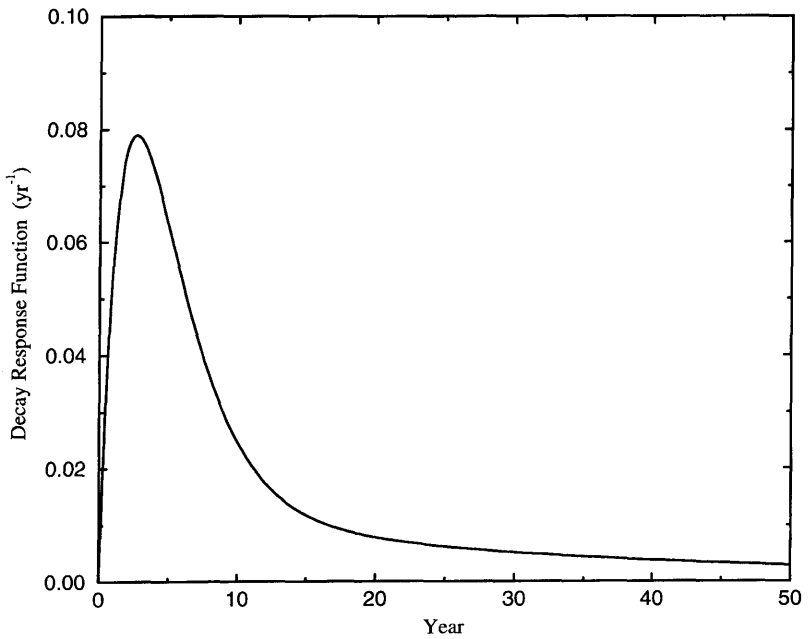

Fig. 8. Decay response function for the 4-box biosphere used in the "Bern" carbon cycle model, i.e., the return flux of carbon into the atmosphere after an initial pulse of carbon assimilation at time $t=0$. The response function is normalized to the pulse size, thus. the integral of the response over time sums to unity.

source in the atmosphere. The use of a mixed-layer pulse response function largely avoids the problem of non-linearities arising from seawater chemistry and gives substantially more accurate results than pulse models based on a atmospheric pulse response function. It should be noted that all carbon cycle models as used here are based on the assumption that the ocean circulation and the natural marine carbon cycle does not vary with time. Further, the interaction of $CaCO_3$ sediments and anthropogenic CO_2 are not included in the models. Accordingly, the results of the full models and their pulse substitute must be viewed with some caution, especially when considering long time scales (> 100 years). Biosphere models, those which have linear decay of assimilated carbon, can also be represented by applying decay response functions in conjunction with an adequate formulation of primary productivity. As pulse models consist of a few equations only, they are simple to implement and run extremly fast, requiring only modest CPU and memory resources. The mixed-layer pulse response function itself provides a simple measure of the surface to deep mixing of a particular ocean model, and mixed-layer responses may thus be used to characterize and compare different ocean models.

The biospheric decay response function represents the timescales describing the overturning of organic material in a particular biosphere model. The turnover of assimilated carbon in the biosphere is one key aspect to determine the amount of carbon sequestered on land as well as the uptake of bomb-produced radiocarbon and the dilution of the fossil fuel ^{13}C signal. To compare different biosphere models and to understand their behaviour it is therefore important to have a simple and standardized measure of this model characteristics. We suggest that the decay response function should be used to characterize and compare the overturning time scales of different biosphere models.

6. Acknowledgement

Before this paper could be completed, we were deeply saddened by the death of our esteemed colleague Uli Siegenthaler. This work is largely based on his ideas. We thank James C. Orr for

providing results of a bomb-radiocarbon simulation carried out with the Princeton model. This work was funded by the U.S. Department of Energy (Grant #DE-FG02–90ER61054), the Swiss National Science Foundation, the European research programme "Global ice sheets during the last two climatic cycles, with an emphasis on entering into glaciation" coordinated by A. Berger, and the Electric Power Research Institute (Grant # RP 3416–01).

7. Appendix

Analytical representation of pulse response functions

We have used a least square fitting procedure (singular value decomposition, Press et al., 1987) to determine analytical expressions for the different pulse response functions to facilitate the construction of mixed-layer pulse response models. As the mixed-layer pulse response functions decrease sharply in the first few years, we were not able to fit the functions accurately by using sums of a few exponentials only. Instead, combinations of polynomial expressions, power law functions, and sum of exponentials are used to represent the pulse response functions and in most cases the pulse response function is broken up into an early and a later period. The response functions are normalized to 1 and the parameter t is in units of years. Additionally, the model parameters needed to build the pulse response model (gas exchange rate, temperature, mixed-layer depth and ocean area) are given in Table 2.

Table 2. *Globally averaged surface temperature, T, gas exchange rate, k_g, and mixed-layer depth, h, for the different models; these values are used in the pulse response models (eqs. (3–6))*

Model	k_g (yr^{-1})	A_{oc} (10^{14} m^2)	h (m)	T (°C)
box-diffusion	1/7.80	3.62	75.0	17.7
HILDA, LS-box	1/9.06	0.84*3.62	75.0	21.4
HILDA, HS-box	1/9.06	0.16*3.62	75.0	1.4
HILDA (LS+HS)	1/9.06	3.62	75.0	18.2
2-D	1/7.46	3.54	50.0	18.3
3-D	1/7.66	3.55	50.9	17.7

A.1. Pulse response function for the HILDA models

The following four pulse response function have been determined by running the full HILDA model. At time equal zero, tracer concentration was initialized to one in the LS or HS-box and to zero everywhere else. The tracer concentrations in the two surface boxes was then monitored through time. Air-sea exchange was set to zero for these two experiments.

A.1.1. $r_{LS}(t)$

for $0<t\leqslant 3.1$ yr:

$$r_{LS}(t) = -0.10481 + 0.23628(t+0.31742)^{-0.45468} + 0.30593(t+0.0074410)^{-0.17084}$$

(check value: $r_{LS}(t=3.1\text{ yr}) = 0.28238$).

for $t > 3.1$ yr:

$$r_{LS}(t) = 0.016538 + 0.15636\times\exp(-t/1.7477) + 0.10521\times\exp(-t/5.4204) + 0.067688\times\exp(-t/16.357) + 0.046700\times\exp(-t/49.521) + 0.036273\times\exp(-t/143.81) + 0.044870\times\exp(-t/383.44)$$

(check value: $r_{LS}(t=3.1\text{ yr}) = 0.28233$).

A.1.2. $r_{HS}(t)$

for $0<t$:

$$r_{HS}(t) = 0.0031494 + 0.016211\times\exp(-t/82.140) + 0.98131\times\exp(-t/1.8255)$$

(check value: $r_{HS}(t=1\text{ yr}) = 0.58658$).

A.1.3. $r_{LS,HS}(t)$

for $0<t\leqslant 28.5$ yr:

$$r_{LS,HS}(t) = \exp(-t/4.0210)\times\{0.00054587 + 0.019389\times t - 0.0051323\times t^2 + 0.0011778\times t^3 - 0.00013873\times t^4 + 0.99349\cdot 10^{-5}\times t^5 - 0.35927\cdot 10^{-6}\times t^6 + 0.58560\cdot 10^{-8}\times t^7\}$$

(check value: $r_{LS,HS}(t=28.5\text{ yr}) = 0.013228$).

for 28.5 yr $< t$:

$$r_{LS,HS}(t) = \exp(-t/192.23) \times \{0.010896 + 0.00014283 \times t + 0.52539 \cdot 10^{-6} \times t^2 - 0.21114 \cdot 10^{-8} \times t^3 + 0.78919 \cdot 10^{-11} \times t^4 - 0.94970 \cdot 10^{-13} \times t^5 + 0.61041 \cdot 10^{-17} \times t^6\}$$

(check value: $r_{LS,HS}(t = 28.5 \text{ yr}) = 0.013233$).

A.1.4. $r_{HS,LS}(t)$

for $0 < t$:

$$r_{HS,LS}(t) = 0.0031652 + 0.00012692 \times \exp(-t/7.0331) - 0.0029104 \times \exp(-t/89.121) - 0.00039938 \times \exp(-t/511.84)$$

(check value: $r_{HS,LS}(t = 100 \text{ yr}) = 0.0018891$).

A.2. Effective mixed-layer pulse response functions

The pulse response function for the Box-Diffusion model has been determined by running the full BD-model. The decrease of the initial tracer perturbation in the surface box due to surface to deep mixing was monitored through time. Air-sea exchange was set to zero. As the BD-model has only one surface box, the pulse response function determined in this way corresponds to an "effective" pulse response function as well.

For the HILDA, 2-D, and 3-D model, the effective pulse response was calculated by solving eq. (3)–(6) for the response function. For these deconvolutions, net air-sea fluxes, $f_{as}(t)$, and atmospheric CO_2 perturbations, $\delta pCO_{2,a}(t)$, were used as obtained by performing an atmospheric pulse experiments with the full models. For the HILDA (Siegenthaler and Joos, 1992) and the 2-D model (Stocker et al., 1994, State A), initial atmospheric CO_2 concentration and the pulse size was 280 ppm. For the 3-D model (Sarmiento et al., 1992), initial atmospheric CO_2 was set to 280 ppm and the pulse size was 265 ppm. In the full 3-D model, perturbation chemistry as defined by eq. (6a) was used for the atmospheric pulse experiments. For the 2-D model, output of the inorganic version (alkalinity = 2302 μeq kg^{-1}) was used; in the HILDA model a buffer function approach is used. Carbon chemistry is defined in the deconvolution routine according to eq. (6a) which is valid up to 300 ppm for temperature around 18 °C and equivalent to eq. (6b) for the range considered. Additional model parameters were set to the values specified in Table 2. It should be noted that the pulse functions provided below should be used in combination with eq. (6b) and the values specified in Table 2.

A.2.1. Box-diffusion model

for $0 < t \leq 3.2$ yr:

$$r_s(t) = 0.14768(t + 0.0026540)^{-0.38810} + 0.34397(t + 0.77514)^{-0.551956}$$

(check value: $r_s(t = 3.2 \text{ yr}) = 0.25459$).

for 3.2 yr $< t$:

$$r_s(t) = 0.019737 + 0.16851 \times \exp(-t/1.6388) + 0.11803 \times \exp(-t/4.8702) + 0.076817 \times \exp(-t/14.172) + 0.050469 \times \exp(-t/43.506) + 0.010469 \times \exp(-t/148.77) + 0.031528 \times \exp(-t/215.71)$$

(check value: $r_s(t = 3.2 \text{ yr}) = 0.25432$).

A.2.2. HILDA model

for $0 < t \leq 2$ yr:

$$r_s(t) = 0.12935 + 0.21898 \times \exp(-t/0.034569) + 0.17003 \times \exp(-t/0.26936) + 0.24071 \times \exp(-t/0.96083) + 0.24093 \times \exp(-t/4.9792)$$

(check value: $r_s(t = 2 \text{ yr}) = 0.32071$).

for 2 yr $< t$:

$$r_s(t) = 0.022936 + 0.24278 \times \exp(-t/1.2679) + 0.13963 \times \exp(-t/5.2528) + 0.089318 \times \exp(-t/18.601) + 0.037820 \times \exp(-t/68.736) + 0.035549$$

$$\times \exp(-t/232.30)$$

(check value: $r_s(t=2\text{ yr})=0.32068$).

A.2.3. 2-D model

for $0<t\leqslant 9.9$ yr:

$$r_s(t)=0.059546+0.12411\times\exp(-t/0.032822)+0.24810\times\exp(-t/0.16254)+0.41432\times\exp(-t/0.75892)+0.15392\times\exp(-t/9.3123)$$

(check value: $r_s(t=9.9\text{ yr})=0.11271$).

for 9.9 yr $<t$:

$$r_s(t)=0.013691+0.067380\times\exp(-t/10.515)+0.036608\times\exp(-t/11.677)+0.026994\times\exp(-t/38.946)+0.026933\times\exp(-t/107.57)+0.012456\times\exp(-t/331.54)$$

(check value: $r_s(t=9.9\text{ yr})=0.11324$).

A.2.4. 3-D model

for $0<t\leqslant 1$ yr:

$$r_s(t)=1.0-2.2617\times t+14.002\times t^2-48.770\times t^3+82.986\times t^4-67.527\times t^5+21.037\times t^6$$

(check value: $r_s(t=1\text{ yr})=0.46630$).

for 1 yr $<t$:

$$r_s(t)=0.014819+0.70367\times\exp(-t/0.70177)+0.24966\times\exp(-t/2.3488)+0.066485\times\exp(-t/15.281)+0.038344\times\exp(-t/65.359)+0.019439\times\exp(-t/347.55)$$

(check value: $r_s(t=1\text{ yr})=0.46664$).

A.3. Biosphere decay response function:

The decay response function of the 4-box biosphere model coupled to HILDA was calculated by solving analyticaly the model equations for the biosphere-atmosphere flux after an initial carbon input into the assimilation reservoirs (ground, wood):

for $0<t$:

$$r_{\text{decay}}(t)=0.70211\times\exp(-0.35t)+0.013414\times\exp(-t/20)-0.71846\times\exp(-55\times t/120)+0.0029323\times\exp(-t/100).$$

(check value: $r_{\text{decay}}(t=5\text{ yr})=0.062610$).

REFERENCES:

Broecker, W. S., Peng, T.-H., Östlund, G. and Stuiver, M. 1985. The distribution of bomb radiocarbon in the ocean. *J. Geophys. Res.* **90,** 6953–6970

Bryan K., Komro, F. G. and Rooth, C. 1983. The ocean's transient response to global surface temperature anomalies. In: Climate processes and climate sensitivity (eds.: Hansen, J. E, Takahashi, T.). *Geophys. Monogr.* **29**, AGU.

Emanuel, W. R., Killough, G. G., Post, W. M. and Shugart, H. H. 1984. Modeling terrestrial ecosystems in the global carbon cycle with shifts in carbon storage capacity by land-use change. *Ecology* **65**, 970–983.

Enting, I. G., Wigley T. M. L. and Heimann, M. 1994. Future emissions and concentrations of carbon dioxide: Key ocean/atmosphere/land analyses. *CSIRO Technical paper no.* **31,** 120pp.

Esser, G. 1987. Sensitivity of global carbon pools and fluxes to human and potential climatic impacts. *Tellus* **39B**, 245–260.

Goyet, C. and A. Poisson 1989. New determination of carbonic acid dissociation constants in seawater as a function of temperature and salinity. *Deep-Sea Res.* **36**, 1635–1654.

Harvey, L. D. D. 1989. Managing atmospheric CO_2. *Clim. Change* **15**, 343–381.

Heimann, M. 1993. The global carbon cycle in the climate system. In: Willebrand and Anderson (eds), NATO ASI Series I, vol. 11. *Modelling ocean climate interactions.* Springer Verlag.

Intergovernmental Panel on Climate Change (IPCC), 1994. Radiative forcing of climate change. In: *Climate Change, 1994.* Cambridge University Press.

Joos, F. 1992. *Modellierung der Verteilung von Spurenstoffen im Ozean und des globalen Kohlenstoffkreislaufes.* Ph.D. Thesis. University of Bern, Bern, Switzerland.

Joos, F., Sarmiento, J. L. and Siegenthaler U. 1991. Estimates of the effect of Southern Ocean iron fertilization on atmospheric CO2 concentrations. *Nature* **349**, 772–774.

Keeling. C. D., Bacastow, R. B. Carter, A. F., Piper, S. C., Whorf, T. P. Heimann, M. Mook,W. G. and Roeloffzen, H. 1989. A three-dimensional model of atmospheric CO_2 transport based on observed winds: 1. Analysis of observational data. In: Aspects of climate variability in the Pacific and Western Americas. Peterson, D. H. (ed.), *AGU Monograph* **55**. Americ Geophysical Union, Washington, 165–236.

Lüdeke M. K. B., Badeck, F. W., Otto, R. D. Häger, C., Dönges, S. Kindermann, J., Würth, G., Lang, T., Jäkel U., Klaudius, A. Ramge, P., Habermehl, S. and Kohlmaier G. H. 1984. The Frankfurt biosphere model: a global process-oriented model of seasonal and long-term CO_2 exchange between terrestrial ecosystems and the atmosphere. I Model description and illustrative results for cold deciduous and boreal forests. *Clim. Res.* **4**, 116–143.

Maier-Reimer, E. and Hasselmann, K. 1987. Transport and storage of CO_2 in the ocean — an inorganic ocean — ciculation carbon cycle model. *Climate Dynamics* **2**, 63–90.

McGuire, A. D., Melillo, J. M., Joyce, L. A., Kicklighter, D. W., Grace, A. L., Moore III B. and Vorosmarty C. J. 1992. Interactions between carbon and nitrogen dynamics in estimating net primary productivity for potential vegetation in North America. *Global Biogeochem. Cycles* **6**, 101–124.

Millero, F. J. 1995. Thermodynamics of carbon dioxide system in the oceans. *Geochim. Cosmochim. Acta* **59**, 661–667.

Oeschger, H., Siegenthaler, U., Schotterer, U. and Gugelmann, A. 1975. A box diffusion model to study the carbon dioxide exchange in nature. *Tellus* **27**, 168–192.

Oeschger, H. and Heimann, M. 1983. Uncertainties of predictions of future atmospheric CO_2 concentrations. *J. Geophys. Res.* **88**, 1258–1262.

Parton, W. J., Schimel, D. S., Cole, C. V. and Ojima, D. S. 1987. Analysis of factors controlling soil organic matter levels in Great Plain grasslands. *Soil Sci. Soc. Am. J* **51**, 1173–1179.

Peng, T.-H., Takahashi, T. and Broecker, W. S. 1987. Seasonal variability of carbon dioxide, nutrients and oxygen in the North Atlantic surface water: observations and a model. *Tellus* **39B**, 439–458.

Press, W. H., Flannery, B. P., Tenkolsky, S. A. and Vetterling, W. T., 1987. *Numerical recipes. The art of scientific computing.* University of Cambridge, Cambridge, 521–528..

Roy, R. N., Roy, L. N., Vogel, K. M., Moore, C. P., Pearson, T., Good C. E., Millero, F. J. and Campbell, D. M. 1993. Determination of the ionization constants of carbonic acid in seawater. *Mar. Chem* **44**, 249–268.

Sarmiento, J. L., Orr, J. C. and Siegenthaler, U. 1992. A perturbation simulation of CO_2 uptake in an ocean general circulation model. *J. Geophys. Res.* **97**, 3621–3645.

Sarmiento, J. L., Le Quéré, C. and Pacala, S. W. 1995. Limiting future carbon dioxide. *Global Biogeochem. Cycles* **9**, 121–137.

Siegenthaler, U. 1993. The uptake of anthropogenic CO_2. Abstract of *4th International CO_2 conference,* Carqueiranne. WMO report no. **89**, WMO, GAW, Geneva, Switzerland.

Siegenthaler, U. and Joos, F. 1992. Use of a simple model for studying oceanic tracer distributions and the global carbon cycle. *Tellus* **44B**, 186–207.

Siegenthaler, U. and Oeschger H. 1978. Predicting future atmospheric carbon dioxide levels. *Science* **199**, 388–395.

Siegenthaler, U. and Oeschger, H. 1987. Biospheric CO2 emissions during the past 200 years reconstructed by deconvolution of ice core data. *Tellus* **39B**, 140–154.

Stocker, T. F., Broecker W. S. and Wright, D. G. 1994. Carbon uptake experiments with a zonally-averaged global ocean circulation model. *Tellus* **46B**, 103–122.

Toggweiler, J. R., Dixon, K. and Bryan K. 1989a. Simulations of radiocarbon in a coarse.resolution world ocean model 1. Steady state prebomb distributions. *J. Geophys. Res.* **94**, 8217–8242.

Toggweiler, J. R., Dixon, K. and Bryan K. 1989b. Simulations of radiocarbon in a coarse.resolution world ocean model 2. Distributions of bomb-produced carbon 14. *J. Geophys. Res.* **94**, 8243–8264.

Wigley, T. M. L. 1991. A simple inverse carbon cycle model. *Glob. Biogeochem. Cycles* **5**, 373–382.